The acoustic pressure generated by the non-spherical collapse of laser-induced cavitation bubbles near a rigid boundary

[1]Silvestre Roberto Gonzalez-Avila* and [1]Claus-Dieter Ohl

[1]*Nanyang Technological University, Singapore, 637371*

Abstract

In this paper we study the acoustic transients emitted during the collapse of a laser-induced cavitation bubble. A 150MHz bandwidth fiber optic probe hydrophone, resolves complex signals produced during the non-spherical collapse of the bubble near a rigid boundary. Simultaneous high-speed video recording up to 200,000 frames/s are correlated with the hydrophone trace. Additionally, we employ an intensified CCD-camera to record snapshots of the shock waves. The acoustic signal contains several pressure peaks with rise times as fast as 18 ns; they correspond to shock waves emitted as the bubble is reaching its minimum volume. For a limited range of standoff parameter values, $1.8 \leq \gamma \leq 5.0$, the strength and time of emission of the first and the second emitted shock waves are related. The maximum radii of the bubbles tested are between 560 μm and 760 μm. We obtain peak pressures of up to 1 kBar during the collapse phase for the bubbles collapsing closes to the boundary.

Keywords: Shock wave; laser-induced bubble; acoustic pressure

Introduction

Acoustic measurements are important in diverse fields of science and engineering; however, the measurements of transient acoustics is not trivial, especially in non-linear acoustic fields, where very fast rise times and high pressures are present. For instance, focused ultrasound waves as those used in lithotripsy peak pressures of a few hundred bars and rise times of less than 50 ns are typically encountered. For this challenge Staudenraus and Eisenmerger [1] developed a fiber optic probe hydrophone (FOPH) that uses the reflected light at the tip of a glass or polymer fiber to deduce the local pressure. Over time this device gained acceptance and became ISO standard to measure intense acoustic fields [2-6], yet it lacks sensitivity. Therefore, to increase the signal-to-noise-ratio averaging of 20 and up to 1000 waveforms has been reported [2]. However, important details varying between experiments which are real and would deserve a closer look may be removed. In this paper we present single acoustic pressure measurements with a FOPH and reveal how the emitted shock waves at the collapse of the bubble depend on γ. Also, we present the pressure developed by single cavitation bubbles that collapse near a solid boundary.

Experimental setup

A schematic diagram of the test section is portrayed in figure 1a. It consists of a modified acrylic cuvette inside which a pulsed laser beam (green Q-switched Nd:YAG laser, pulse duration 6 ns) is focused to create single cavitation bubbles at specific locations from a solid boundary. The optical arrangement is similar to a setup previously reported [7]; however, in the current setup we sample a small portion of the laser beam energy, ~4%, to accurately detect the time when the laser beam appears. The rising signal from the photo diode (see figure 1a) triggers the data acquisition by the oscilloscope (LeCroy HRO64Zi 2GHz 12-Bit) and the pressure generated during the cavitation event is recorded by a fiber optic probe hydrophone, FOPH (690 ONDA, 150 MHz bandwidth). The 125 μm tip of the fiber was inserted into the test section through a small hole of 0.6 mm in diameter, and positioned with a 3-axis stage at a distance *d* from the bubble inception location. A pulse delay generator (Berkley Scientific, BNC model 575) triggers and synchronizes the laser and the high-speed camera (Photron SAX-2) coupled to a 60 mm macro lens (Nikor) at full magnification (resolution 20 um per pixel). The scene is illuminated with mildly diffused light from a LED fiber optic lamp (REVOX SLG 150V). The shockwaves emitted during the bubble expansion or collapse are recorded with an intensified 12 bit CCD camera (PCO Dicam Pro). With this camera single images with a minimum exposure time down to 3ns can be captured. There we increase the spatial resolution to 2.2 μm/pixel by coupling the camera to a long distance microscope (Infinity CF-4). A circular aperture placed in front of a light emitting diode (Cree CBX 1512) was used for illumination and to record shadowgraphs of the emitted shock waves.

*Corresponding Author, S. Roberto Gonzalez-Avila: roberto_glez83@hotmail.com

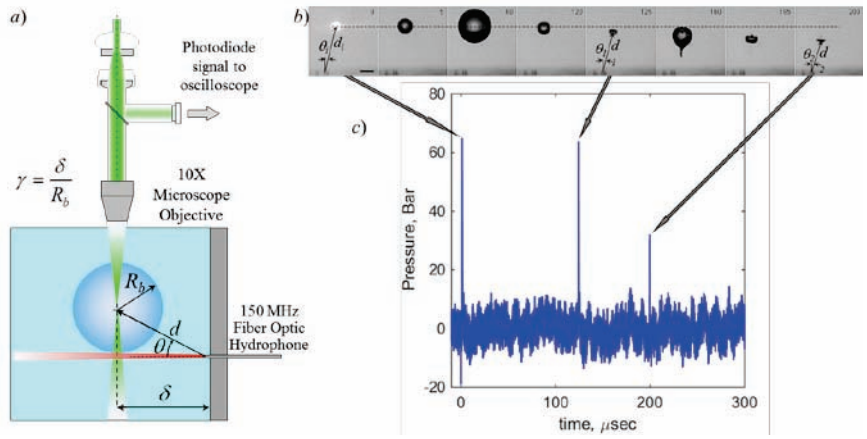

Figure 1. (a) Experimental setup and experimental parameters; (b) Laser-induced cavitation bubble created near a solid wall; the laser beam appears from right to left; the fiber optic can be seen in the lower left side of each frame, $\gamma = 2.7$; $R_b = 616$ μm. The length of the bar in the lower right corner of the first image is 500 μm; time is in μs. The dotted black is added as an aid to the eye; (c) the acoustic signal recorded by the FOPH; the three prominent peaks from left to right correspond to the bubble's inception, bubble's first collapse and the bubble's second collapse, respectively; $d_i = 1.7$ mm; $d_1 = 1.5$ mm; $d_2 = 1.2$ mm; $\theta_i = 13°$; $\theta_1 = 14°$; $\theta_2 = 17°$.

Figure 2b displays selected frames from a high-speed recording, $\gamma = 2.7$ and $R_b = 616$ μm; the images are rotated 90° clockwise. From left to right they depict the bubble dynamics from inception to the second collapse. The high-speed camera and the FOPH were triggered simultaneously, thus the images can be correlated to the acoustic trace. The dotted black line guides the eye to emphasis the translation of the cavitation bubble towards the boundary in its first and second collapse. The acoustic trace, figure 2c, shows three distinct pressure peaks; from left to right the first peak is due to the shockwave emitted during the nucleation of the cavitation bubble; the second and third peaks are due to the shock waves emitted during the first and second collapse of the bubble, respectively. During bubble expanding and before reaching its minimum volume, $5 \leq t \leq 120$ μs no pressure peaks or any other prominent features in the acoustic trace are observed. Also, after the bubble reaches its minimum volume no other peak is detected; only around the time the second collapse takes place a third peak is visible in the graph.

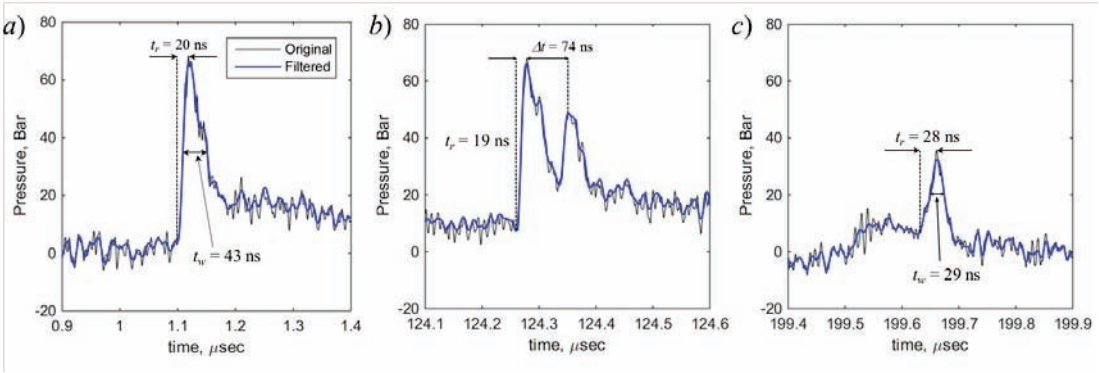

Figure 2. Close up of the acoustic pressure peaks portrayed in figure 1c. (a) inception; (b) bubble's first collapse; (c) bubble's second collapse.

The peaks from figure 1c are zoomed in, see figure 2a-c. Notice that these curves are essentially compression waves and do not show a tensile component which is different from previous measurements [5,6]. Interestingly, the rise time is only 20 ns and the width of the peak about 43 ns. Figure 2b shows an interesting feature which becomes visible at high temporal resolution during the first bubble collapse. The acoustic trace consists of two peaks emitted with a time delay of only 74 ns. We believe these two peaks are due to the non-spherical bubble collapse. Figure 2c also displays a short peak that is correlated to the time of the second collapse of the bubbles. These figures, 2a-c, present two traces each, the light color trace is the original acoustic signal recorded, while the darker trace is the signal after high frequency components (>70 MHz) have been removed.

Thus, to get a better evaluation of the peak pressure developed on the wall during cavitation bubble collapses, it is first necessary to evaluate the variation of the peak pressure measured as a function of the angular position θ and distance d. Figure 3a displays the change in the peak pressure detected with angular position θ. Each dot is a single event; in these tests both the maximum bubble size, R_b, and the distance between the bubble's inception location and the fiber tip, d, were kept constant (within experimental uncertainty); the red circles plot the peak pressure as a function of incidence angle of the shock wave with the fiber tip, d = 1.68 ± 0.02 mm; the FOPH trace is recorded synchronously with the high-speed video images, thus we can clearly obtain the maximum size obtained by the bubble. For the lower lower data points (blue squares) in figure 3a the CCD camera was used. It was synchronized to capture the shock wave as it arrives at the fiber tip for the different γ values tested. The inset in the lower left corner of figure 3a depicts a sample image; the distance between the bubble's inception location and the fiber tip is d = 1.00 ± 0.01 mm; the pressure is adjusted to a pressure of d = 1.68 mm. For these tests the time at which the first pressure peak is detected, T_c, is used to estimate the bubble size with $R_b = T_c(P_\infty/\rho)/1.83$; the average bubble size of the tests is 520 ± 6 μm. Figure 3b portrays the variation of maximum pressure with distance d; the parameter d was measured by locating the centroid of the plasma and the tip of the fiber for each test; snapshots of the plasma are shown,,too . In these tests a single cavitation bubble is created 2.6 mm away from the tip of the fiber optic then the fiber is moved closer to the inception location and both high-speed video and the acoustic signal are recorded. The figure portrays the peak pressure detected by the FOPH during this process. The angle formed by the axis of the fiber and the nucleation site, θ, was fixed at 15 ± 1° together with the laser energy resulting in bubbles of R_b = 695 + 16 μm (average of 36 cavitation events). The distance between the fiber tip and the nucleation site, d, varied in the range 0.27 mm ≤ d ≤ 2.6 mm. In the linear regime an inversely proportional decay of the wave amplitude with distance (1/d decay) is expected [8] as confirmed by the data in figure 3b.

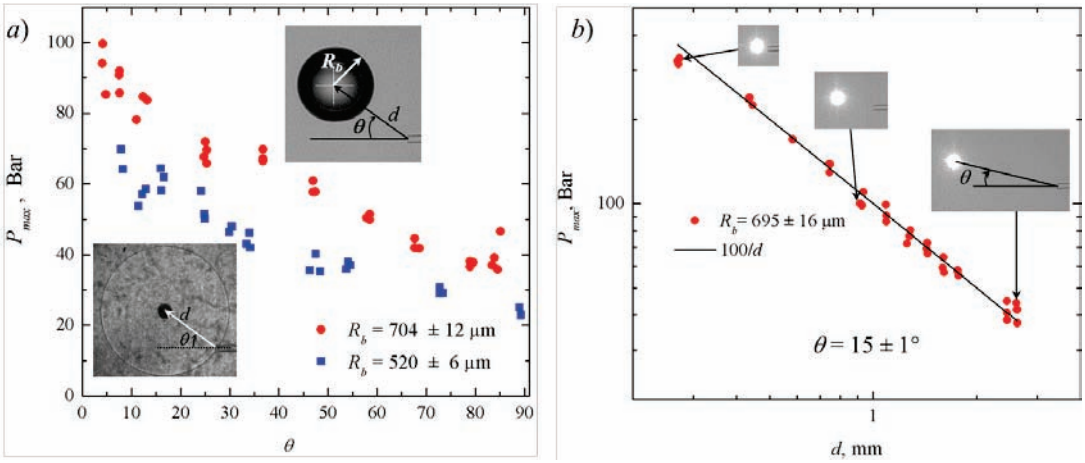

Figure 3. (a) Change of peak acoustic pressure with angular position; (b) Change of peak acoustic pressure with distance from the fiber tip

The prime motivation for this work was to study the pressure generated by the collapse of a single bubble near a solid wall. Here we find interesting acoustic traces for certain ranges of γ values. In the range 1.8 ≤ γ ≤ 5.0 up to *three* distinct pressure peaks were detected during the bubble collapse. The third peak is usually weaker and more difficult to detect thus we focus here on the features of the first and second pressure peaks of the first bubble collapse. Samples (non-averaged) for increasing γ are shown in figures 4a-d. For γ = 1.9 the rise time of the first peak is comparably large, t_r = 72 ns. Yet, for larger stand-off distances the pressure rises within less than 30 ns. Additionally, the variation of the ratio of the first pressure peak, P_1, to the second pressure peak, P_2, with γ and the time delay between them, Δt changes as a function of γ. In figure 4a the magnitude of the first pressure peak is ~50% that of the second peak; both pressure peaks display approximately the same magnitude in figure 4b and in figure 4c the amplitude of the first peak is more than twice that of the second peak. From γ = 4.9 on a single peak is resolved, figure 4d which is consistent that Δt decreases with γ.

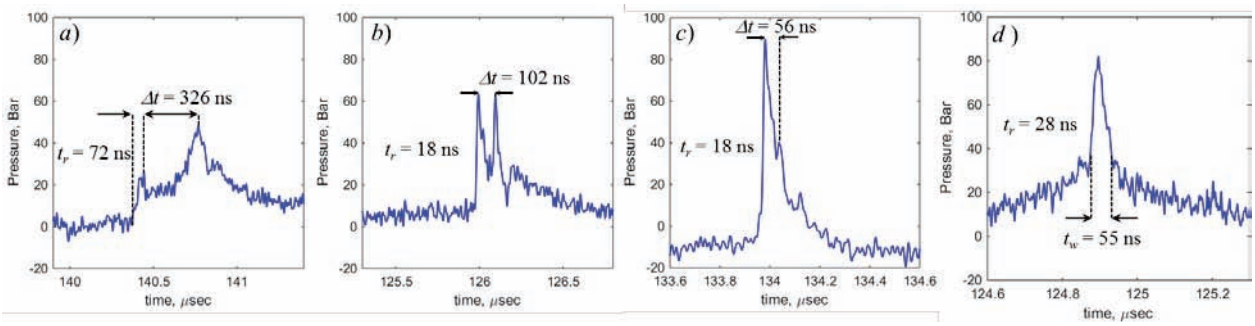

Figure 4. Pressure peaks detected at the first collapse of a cavitation bubble; a) $\gamma = 1.9$, $R_b = 677$ μm; b) $\gamma = 2.5$, $R_b = 620$ μm; c); $\gamma = 3.0$, $R_b = 679$ μm; e) $\gamma = 4.9$, $R_b = 701$ μm.

Unfortunately, the high-speed camera does not allow us to visualize the shock waves emitted either at the inception or at the collapse of the bubble we therefore use the single frame ICCD camera with a 3ns exposure time. Figure 5a displays two circles in the lower left corner of the image; the outer circle has a radius $R_o = 183$ μm, while the smaller circle has a radius $R_i = 108$ μm. Assuming constant speed of sound at 1480 m/s the estimated time delay between in the emission of the shock waves is Δt = 50ns which nicely fits with the time between the pressure peaks shown in figure 5b of the event, $\gamma \sim 2.3 \pm 0.2$. Vogel and Lauterborn (1988) and more recently by Supponen et al. (2107) have reported the emissions of multiple shock waves from a single bubble collapse have. Next, we want to demonstrate that the timing and strength emission of the first and the second shock waves are very well reproducible and how they depend on γ.

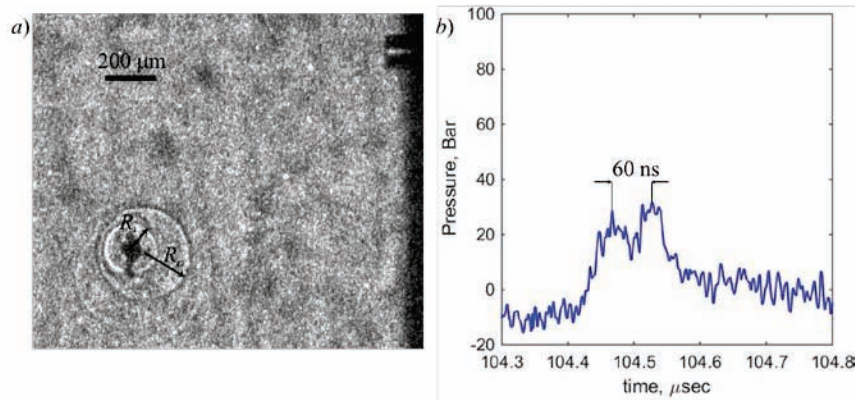

Figure 5. (a) Acoustic transients emitted at the collapse of the cavitation bubble, g ~ 2.3, exposure time is 3 ns; b) the acoustic signal recorded by the FOPH around the time reaches its minimum volume.

Therefore, we have extracted from many experiments the ratio of the first to the second pressure peak, and the time delay between these two peaks, Δt, and graphed them as a function of γ in figures 6a-b. In figure 6a this relationship between the P_{jet}/P_{tip} ratio with γ is clearly observed up to $\gamma \approx 1.8$, below the amplitudes were too weak to discern them. In the range $1.8 \leq \gamma \leq 3.0$, there is a increase of P_{jet}/P_{tip} with γ. The final stage of the collapse of a cavitation bubble is too fast to be resolved with our imaging system. However, a possible explanation for the change in the strength of the pressure peaks is as follows: The first pressure peak occurs due to the impact of the jet on the opposite wall of the bubble (see Ohl et al 1999). For the lower γ tests $1.8 \leq \gamma \leq 2.5$ the jet penetrates the bubble early in the collapse phase, thus the opposite wall has not gained enough velocity. As the jet impacts later in the collapse phase at slightly larger γ values the opposite wall of the bubble is moving faster and the water hammer pressure upon impact of the jet with the opposite bubble wall is stronger and the jet shock wave, P_{jet}, increases. Around $\gamma = 2.5 \pm 0.1$ the strength of the shocks are approximately the same and the ratio is maximum at $\gamma = 3.0 \pm 0.1$. As the jet develops later during in the collapse phase the collapse of the bubble occurs quasi-spherically and the shocks may

not be discernible or (unlikely) as single shock being emitted. With respect to the time delay between the shock waves at the lower γ values the collapse of the bubble is more deformed, then not only the jet pierces sooner in the collapse phase but also the volume trapped between the tip of the jet and the opposite wall of the bubble continues to compress until a second shock wave, the tip bubble shock wave, P_{tip}, is emitted. For larger γ values the collapse becomes more symmetric thus the jet pierces at a later stage in the collapse of the bubble, and the small volume trapped cannot compress much further, hence the time delay between the first and the second shock wave is shorter than during collapse at lower γ [11].

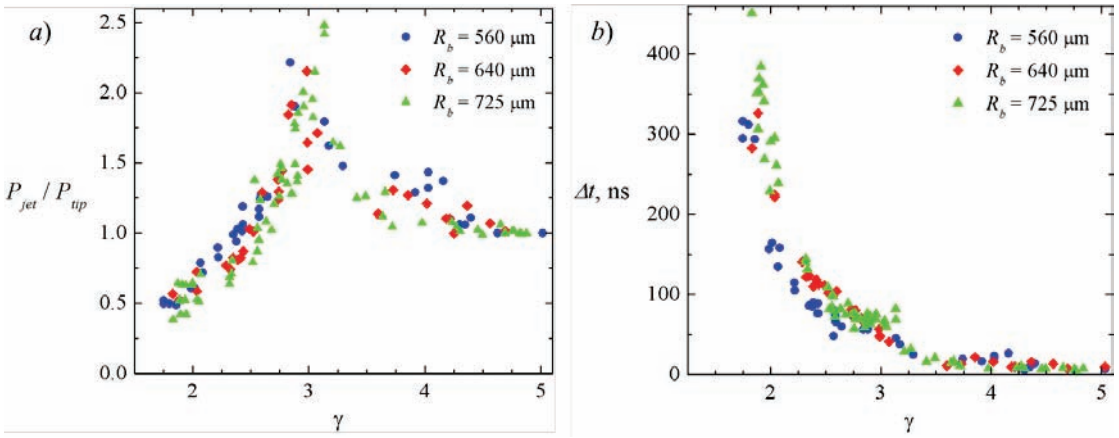

Figure 6. (a) The ratio of the peak pressures P_{jet}/P_{tip} from the cavitation bubble collapse with stand-off parameter; b) time delay, Δt, between the emission of the jet shock wave, P_{jet} and the tip bubble shock wave, P_{tip}.

Finally, a summary of the tests conducted near the solid boundary, $0.1 \leq \gamma \leq 3.0$, is portrayed in figure 7. In figure 7a the original peak pressure detected is shown; in figure 7b the pressure at the location where the bubble collapse takes place is portrayed; the original pressure values are corrected for distance and the angle of incidence, θ. The data in figure 7b shows more variation than the original data in figure 7a because the distance from the fiber tip to the bubble was different for different tests. In some cases the minimum volume detected corresponded to a torus while in other cases the minimum volume captured was quasi spherical. Already bubbles of sub-millimeter size can generate pressures on the boundary of up to 1 kBar for a few ns. Also, notice that for $\gamma \sim 0.9$ the sound emission decreases significantly; this is in good agreement with previous observations [13,14,10]. This is a consequence of the alteration of the bubble collapse due to the presence of the boundary and the formation of a vortex ring.

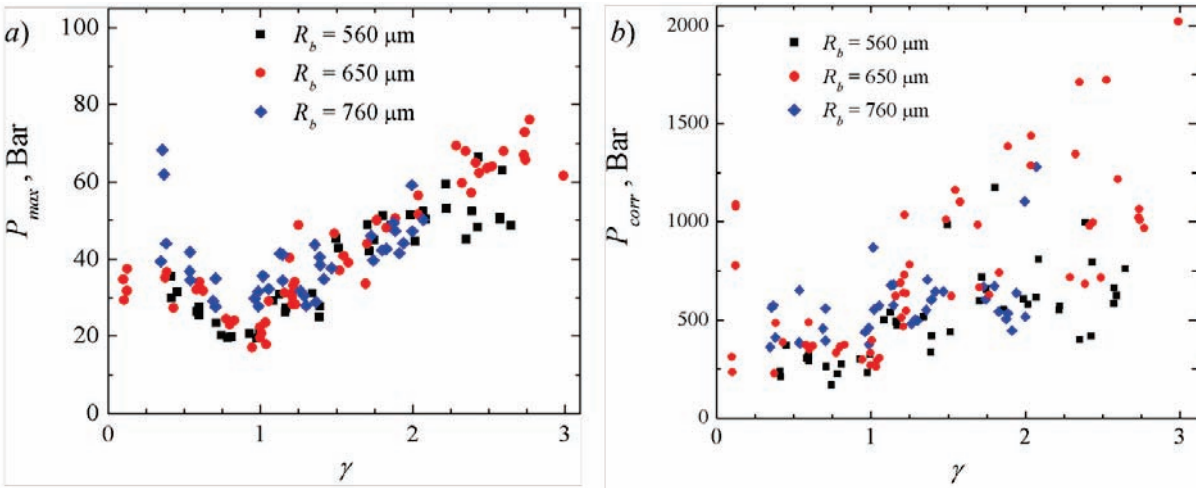

Figure 7. The acoustic pressure near the cavitation bubble at its first collapse; a) the peak pressure measured; b) the corrected peak pressure for distance and angular position at its first collapse, P_{corr}.

For larger γ values where the collapse is quasi spherical the involution of the bubble takes place approximately in a radial fashion thus the pressure peaks emitted are strong; however, when the bubble collapses close to a boundary, $\gamma \sim 0.9$, the jet penetrates through it before it has reached its minimum volume. As the jet impact on the wall it spreads radially transferring kinetic energy into circulation, forming a system of vortex rings. There the compression of the bubble content is less violent and sound emission diminished [15]. Figure 7a depicts how the acoustic emission decreases for $\gamma = 0.9$.

Conclusion

We have presented single acoustic pressure measurements of the acoustic transients emitted during the non-spherical collapse of laser-induced cavitation bubbles near a rigid boundary. The data is recorded for a range of stand-off parameters, far from the boundary, $\gamma \sim 5$, down to the collapse next to the boundary, $\gamma = 0.1$. The results show that strength of the shock waves emitted, namely the shock wave emitted due to the jet impact on the opposite wall of the bubble, P_{jet} and the tip bubble shock wave, P_{tip}, are a complex but comprehensible function in the range $1.8 \leq \gamma \leq 5.0$. This information we think is suitable for comparison with simulations to unravel the interaction leading to cavitation induced material damage.

Acknowledgements

We appreciate funding through ONR under grant number Grant No. N62909-16-1-2139.

References

[1] Stadenraus, J.,Eisenmenger, W. (1993). *Fiber-optic probe hydrophone for ultrasonic and shock wave measurements in water.* Ultrasonics, 31(4).
[2] Wang, Z. Q., Pecha, R., Gompf, B., Eisenmenger, W. (1999). *Single bubble sonoluminescence: Investigations of the emitted pressure wave with a fiber optic probe hydrophone*, Phys Rev-E, 59(2).
[3] Sankin, G. N., Simmons, W. N., Zhu, S. L., Zhong, P. (2005). *Shock Wave Interaction with Laser Generated Single Bubbles*. Phys Rev Lett, 95, 034501.
[4] Sankin, G. N., Zhong, P. (2006). *Interaction between shockwave and single inertial bubbles near an elastic boundary*. Phys Rev E, 74, 046304.
[5] Sankin, G. N., Zhou, Y., Zhong, P. (2008). *Focusing of shock waves induced by optical break down in water*. J. Acoust. Soc. Am. 123 (6).
[6] Zijlstra, A., Ohl, C-D. 2007. *On fiber optic hydrophone measurements in a cavitating liquid*. J Acoust Soc Am., 123, 29-32.
[7] Gonzalez-Avila, S. R., OHL, C-D. (2106). *Fragmentation of acoustically levitating droplets by laser-induced cavitation bubbles*. J. Fluid Mech. 805.
[8] Cole, R. H. (1948). *Underwater Explosions*. Princeton University Press.
[9] Ohl, C-D., Kurz, T., Geisler, R., Lindau, O., Lauterborn, W. (1999) *Bubble dynamics, shock waves and sonoluminescence*. Phil. Trans. R. Soc. Lond. A. 357.
[10] Vogel, A., Lauterborn, W. (1988). *Acoustic transient generation by laser-produced cavitation bubbles near solid boundaries*. J Acoust. Soc. Am.84 (2).
[11] Supponen, O., Obreschkow, D., Kobel, P., Tinguely, M., Dorsaz, N., Farhat, M. (2017). *Shock waves from nonspherical cavitation bubbles*, Phys Rev Fl, 2, 093601.
[12] Lindau, O., Lauterborn, W. (2003). *Cinematographic observation of the collapse and rebound of a laser-produced Cavitation bubble near a wall*. J Fluid Mech. 479.
[13] Naudé, C. F., Ellis, A. T., (1961). *On the Mechanism of Cavitation Damage by Nonhemispherical Cavities Collapsing in Contact With a Solid Boundary*, J Basic Eng. 83 (4).
[14] Tomita, Y., Shima, A. (1986). *Mechanisms of impulsive pressure generation and damage pit formation by bubble collapse*. J. Fluid Mech., 169.
[15] Chahine, G. L., Genoux, P. F., (1983). *Collapse of a Cavitaing Vortex Ring*. Trans. ASME J. Fl Eng, 105 (4).